MOLECULAR IMAGING AND BIOLOGY

Published Online: 13 May 2010

Mol Imaging Biol (2011) 13:53–58
DOI: 10.1007/s11307-010-0332-y

RESEARCH ARTICLE

In Vivo Mouse Bioluminescence Tomography with Radionuclide-Based Imaging Validation

Yujie Lu,[1] Hidevaldo B. Machado,[2] Qinan Bao,[1] David Stout,[1] Harvey Herschman,[1,2] Arion F. Chatziioannou[1]

[1]*Crump Institute for Molecular Imaging, Department of Molecular and Medical Pharmacology, David Geffen School of Medicine at UCLA, Los Angeles, CA 90095, USA*
[2]*Department of Biological Chemistry, Molecular Biology Institute, University of California, Los Angeles, CA 90095, USA*

Abstract

Introduction: Bioluminescence imaging, especially planar bioluminescence imaging, has been extensively applied in *in vivo* preclinical biological research. Bioluminescence tomography (BLT) has the potential to provide more accurate imaging information due to its 3D reconstruction compared with its planar counterpart.

Methods: In this work, we introduce a positron emission tomography (PET) radionuclide imaging-based strategy to validate the BLT results. X-ray computed tomography, PET, spectrally resolved bioluminescence imaging, and surgical excision were performed on a tumor xenograft mouse model expressing a bioluminescent reporter gene.

Results: With different spectrally resolved measured data, the BLT reconstructions were acquired based on the third-order simplified spherical harmonics (SP3) approximation and the diffusion approximation (DA). The corresponding tomographic images were obtained for validation of bioluminescence source reconstruction.

Conclusion: Our results show the strength of PET imaging compared with other validation methods for BLT and improved source localization accuracy based on the SP_3 approximation compared with the diffusion approximation.

Key words: Optical molecular imaging, Bioluminescence imaging/tomography, Imaging validation, Reconstruction algorithm

Introduction

Optical molecular imaging, especially planar bioluminescence and fluorescence imaging, has been extensively applied in preclinical research, particularly with small animal models such as genetically modified mice and murine tumor xenografts. Tomographic optical molecular imaging localizes the source position and should provide more accurate biological information compared to its planar counterpart [1]. The possibility and potential of bioluminescence tomography (BLT) [2, 3] and fluorescence molecular tomography as standalone imaging modalities have been investigated using phantoms and mouse experiments [4, 5]. To develop a practical, accurate, and robust BLT system, more factors need to be investigated, such as *in vivo* validation strategies and more precise reconstruction algorithms among others. To validate the optical source information, physical and *in vitro* methods are commonly used in phantom- and nonbiological mouse-based experiments. *In vivo* imaging strategies, such as computed tomography (CT), are also used to validate artificial source-based optical experiments [6]. Due to the poor soft tissue contrast in preclinical CT imaging, it is difficult to identify the optical source *in vivo* based on anatomical information only. New *in vivo* validation strategies are necessary to develop tomographic optical molecular imaging. In the transition from phantom-based feasibility investigations

Correspondence to: Arion F. Chatziioannou; *e-mail:* archatziioann@mednet.ucla.edu

to *in vivo* biological research, several assumptions affect source reconstruction quality [7]. Although the diffusion approximation (DA) has been widely used, the method becomes inaccurate when the bioluminescence sources are near the surface, or in tissues with high and anisotropic absorption [7, 8]. This inaccuracy leads to reduced information acquired from bioluminescence sources. Reconstruction algorithms based on high-order approximations to the radiative transfer equation (RTE) should improve these results and need to be further developed [8]. In addition, *a priori* information, such as spectrally resolved measurements [9, 10] and permissible source region [11], is indispensable to constrain the possible solutions in BLT reconstruction.

In this paper, an *in vivo* validation strategy based on positron emission tomography (PET) is proposed for tomographic bioluminescence imaging. An *in vivo* mouse experiment was performed with a luciferase-based tumor xenograft. After acquiring multiple spectral optical data, the bioluminescence source was localized with SP_3- and DA-based reconstruction algorithms and compared to PET and CT acquired data. The reconstructed results not only show the advantages of PET-based *in vivo* validation compared with traditional CT-based methods but also demonstrate the effectiveness and potential of the SP_3-based BLT reconstruction algorithm.

Materials and Methods

In the experiment, three types of imaging modalities, that is, X-ray CT, PET, and optical imaging, were used. To maintain the animal in the same position throughout the whole procedure, a glass holder was fabricated to support the mouse. To realize multi-view detection, two mirrors were used to acquire the photon distribution from two side views. A murine tumor cell line, MC38fluc, transfected to provide constitutive expression of firefly luciferase, was used to generate a tumor xenograft in the abdomen of a nude mouse and allowed to develop for 3 weeks. To perform the imaging experiments, the animal was anesthetized and injected with the optical substrate (luciferin). Optical data was gathered 10 min after substrate administration using the Maestro 2 *in vivo* Imaging System (CRI, Woburn, MA, USA). The filter bandpass width was set to 20 nm, and optical data at four wavelengths (600, 620, 640, and 660 nm) was collected. The exposure time for each wavelength was 5 min. Fig. 1a shows a mouse photograph and the corresponding optical data at 660 nm. The image signal-to-noise ratio (SNR) ranged from 6.81 to 7.27 (SNR was calculated by S_{avg}/N_{avg} at four wavelengths, where S_{avg} and N_{avg} are the averages of the image signal and noise). Since the optical signals are weak and the sensitivity of this particular detection system is low, the image SNR is low. However, the nature of the optical filter [12] allowed the photon distribution on the mouse surface to be observed for arbitrary wavelength bands. Because the tumor position after 3 weeks was very close to the mouse abdomen, the photon distribution could not be acquired from the two side views. After finishing the bioluminescence optical signal acquisition, the PET tracer (^{18}F-fluorodeoxy-glucose (^{18}F-FDG)) was injected intravenously into the mouse. After 1 h uptake, the animal was imaged using a microCT and a high resolution preclinical PET system (Siemens Preclinical Solutions, Knoxville, TN, USA) to obtain the CT and PET images shown in Fig. 1b, c. Localization of the tumor position from the PET images is facilitated due to the high ^{18}F-FDG uptake compared to background. However, the same is not true when analyzing the CT images due to the similar density contrast between the tumor and other tissues in the animal abdomen. These data clearly show the advantages of PET imaging for *in vivo* optical imaging validation. After all the collection of the imaging data, the mouse was euthanized and dissected to confirm the tumor location. A tumor mass of approximately 3 mm diameter was found attached to the small intestine, shown in Fig. 1d. To realize the spectrally resolved BLT reconstruction with the high-order approximations to the RTE, we have developed a fully parallel reconstruction framework with the simplified spherical harmonics approximation (SP_N) [13]. Regarding the SP_3 approximation, its mathematical model and boundary formula are [14]

$$\begin{cases} -\nabla\cdot\frac{1}{3\mu_{a1}}\nabla\varphi_1+\mu_a\varphi_1-\left(\frac{2}{3}\mu_a\right)\varphi_2=S \\ -\left(\frac{2}{3}\mu_a\right)\varphi_1-\nabla\cdot\frac{1}{7\mu_{a3}}\nabla\varphi_2+\left(\frac{4}{9}\mu_a+\frac{5}{9}\mu_{a2}\right)\varphi_2=-\frac{2}{3}S \end{cases} \quad (1)$$

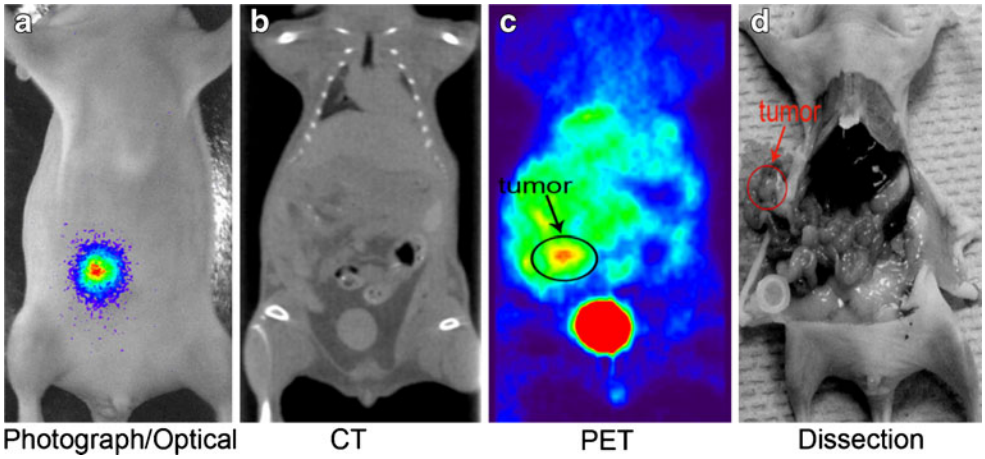

Fig. 1. Imaging of a xenograft tumor in a nude mouse. The photograph is used to map the optical data from the CCD camera onto the surface of the volumetric mesh; the computed tomography slice shows the same position cross-section with the positron emission tomography scan; dissection is used to further confirm the tumor position.

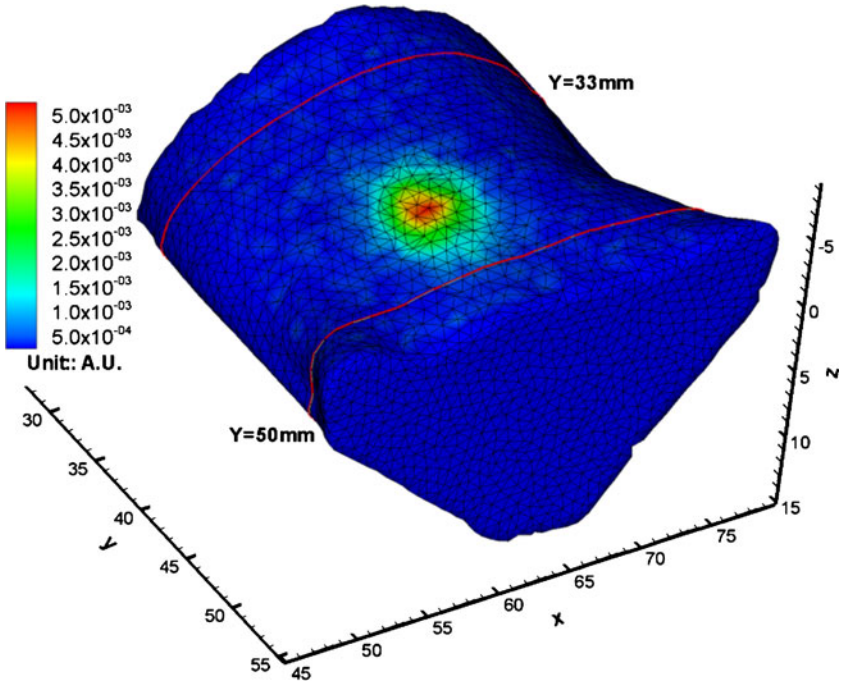

Fig. 2. The volumetric mesh used in bioluminescence tomography reconstruction and the photon distribution at 660 nm. The *red lines* are used to show the permissible source region.

$$\begin{cases} \left(\frac{1+B_1}{3\mu_{a1}}\right)\upsilon\cdot\nabla\varphi_1 - \left(\frac{D_1}{\mu_{a3}}\right)\upsilon\cdot\nabla\varphi_2 = -\left(\frac{1}{2}+A_1\right)\varphi_1 + \left(\frac{1}{8}+C_1\right)\varphi_2 \\ -\left(\frac{D_2}{\mu_{a1}}\right)\upsilon\cdot\nabla\varphi_1 + \left(\frac{1+B_2}{7\mu_{a3}}\right)\upsilon\cdot\nabla\varphi_2 = \left(\frac{1}{8}+C_2\right)\varphi_1 - \left(\frac{7}{24}+A_2\right)\varphi_2 \end{cases} \tag{2}$$

where $\mu_{an}=\mu_s(1-g^n)+\mu_a(n=1, 2, 3)$, $\varphi_i(i=1, 2)$ are the composite moments relevant to the Legendre moments, μ_s and μ_a are the scattering and absorption coefficients, and S is the bioluminescence source. Note that μ_{an}, φ_i, and S depend on the wavelength when spectrally resolved measured data is acquired. The coefficients $A_1,...,D_1,...,A_2,...,D_2$ can be calculated using the formulas in [14]. Furthermore, the exiting partial current J^+ on the mouse surface is obtained:

$$\begin{aligned} J^{+,b} = \left(\frac{1}{4}+J_0\right)\left(\varphi_1 - \frac{2}{3}\varphi_2\right) - \left(\frac{0.5+J_1}{3\mu_{a1}}\right)\upsilon\cdot\nabla\varphi_1 \\ +\frac{1}{3}\left(\frac{5}{16}+J_2\right)\varphi_2 - \left(\frac{J_3}{7\mu_{a3}}\right)\upsilon\cdot\nabla\varphi_2 \end{aligned} \tag{3}$$

where the coefficients $J_0,...,J_3$ can also be calculated based on the relevant formulas in [14]. Note that SP_1 (DA) can be obtained correspondingly by setting $\varphi_2=0$. After a series of deductions, a simple relationship between the measurable boundary data and the unknown source distribution is established:

$$J^{+,b} = AS^p \tag{4}$$

Table 1. Optical properties of actual mouse muscle [7]

Wavelength	600 nm	620 nm	640 nm	660 nm
$\mu_a(\lambda)$ (mm^{-1})	0.187	0.107	0.088	0.08
$\mu_s(\lambda)$ (mm^{-1})	9.29	9.22	9.13	9.02

where

$$J^{+,b} = \begin{bmatrix} J^{+,b}(\lambda_1) \\ \vdots \\ J^{+,b}(\lambda_k) \\ \vdots \\ J^{+,b}(\lambda_K) \end{bmatrix}, A = \begin{bmatrix} \gamma_1 G(\lambda_1) \\ \vdots \\ \gamma_k G(\lambda_k) \\ \vdots \\ \gamma_K G(\lambda_K) \end{bmatrix}$$

where K is the number of the used wavelengths, γ_k is the percentage at the wavelength λ_k of the total energy, and $G(\lambda_k)$ is the relationship matrix between the permissible source region S^p and the measurable data $J^{+,b}$ at the wavelength λ_k. The surface measured data $J^{+,m}$ corresponding to $J^{+,b}$ leads to a reconstruction failure when solving Eq. 4 directly due to the presence of noise. We can solve the bound-constrained least squares problem

$$\min_{0<S^p<S^{sup}} \Theta(S^p) : ||AS^p - J^{+,m}||^2 \tag{5}$$

where S^{sup} is the upper bound of the source density. By minimizing the objective function $\Theta(S^p)$, BLT reconstruction becomes possible. Here, the limited memory variable metric bound-constrained quasi-Newton method (BLMVM) is used for BLT reconstruction [15].

Results

With respect to the photon distribution on the mouse surface, the volumetric mesh of half the mouse body shown in Fig. 2 was generated using the commercial software Amira 3.0 (Mercury Computer Systems, Inc. Chelmsford, MA, USA). Since the photon distribution can only be obtained from the ventral view and the photon propagation path is almost totally consisted of muscle tissue, we assumed that the reconstructed domain was homogeneous with muscle tissue.

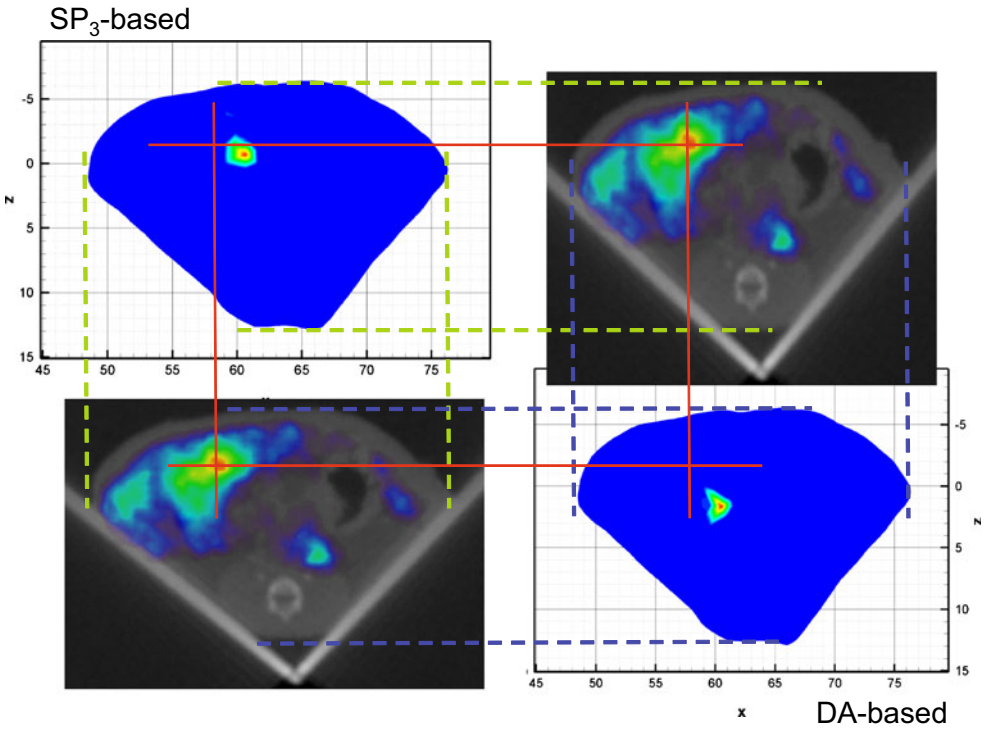

Fig. 3. Imaging validation and bioluminescence tomography reconstruction comparison between SP_3- and DA-based models. The *dashed lines* are used to align the boundaries of optical cross-sections with the corresponding computed tomography slices; the *red lines* show the center of tumor on positron emission tomography images.

The mesh contained about 10,000 discretized points with the average element of 1.2 mm diameter. The assumed optical properties of mouse muscle are shown in Table 1. To constrain the BLT solution, a permissible source region with 5,965 discretized points was selected, that is $S^p = \{(x,y,z) | 33.0 < y < 55.0 \text{ mm}, (x,y,z) \in \Omega\}$, where Ω is the entire domain, as shown in Fig. 2. The acquired optical data was mapped onto the mesh surface after manual co-registration between the mesh and the mouse photograph in Amira. The differences of the optical properties at different wavelengths

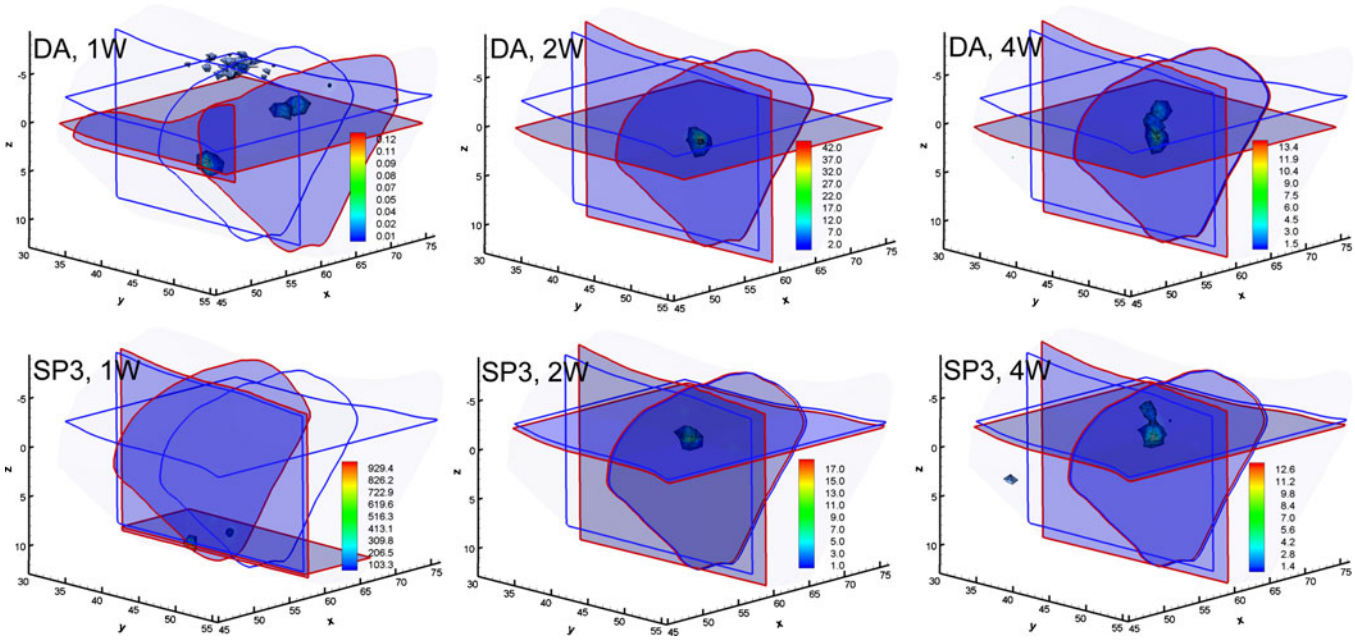

Fig. 4. DA- and SP_3-based bioluminescence tomography reconstruction comparisons with different spectrally resolved measurements. *1W*, *2W*, and *4W* denotes that one (660 nm), two (600 and 660 nm), and four wavelengths are used. Cross-sections with *blue* and *red boundaries* are the center position of the actual and reconstructed sources, respectively. The volumetric mesh denotes reconstructed values larger than 10% of the reconstructed maximum.

improve the BLT reconstruction quality. Since the optical properties at 600 and 660 nm have a large difference (as shown in Table 1), Fig. 3 shows the SP_3- and DA-based reconstruction results when using 1,072 measured points and these two wavelengths. Through comparison between optical and PET reconstructed results, one can determine that the source location errors of SP_3-based reconstruction are less than 1.5 mm at each direction. However, the DA-based BLT reconstruction is not as accurate. In the depth direction, the location errors are about 4 mm. Note that the background noise is very high due to nonspecific probe uptake in PET imaging. This reconstruction comparison shows the effectiveness of the SP_3-based reconstruction algorithm for BLT. To further confirm the effect of spectrally resolved measured data, BLT reconstructions using measurements in one and four wavelengths were performed. The reconstructed results are shown in Fig. 4. Due to the absence of source depth information when using one wavelength, poor reconstruction results were obtained. However, when four wavelengths were used, the localization of the source center was not improved; instead, there were some artifacts in the reconstructed results compared with two wavelengths. Small differences in the optical properties between 620, 640, and 660 nm reduced the benefits from multispectral measured data, while the noise effects in the measured data became significant. Although the use of multispectral data can improve reconstructed image quality, in principle, the results are a trade-off between photon sensitivity (presence of statistical noise) and differences between optical properties.

Discussions and Conclusion

To the best of the authors' knowledge, this contribution represents the first time that PET imaging has been used for *in vivo* BLT imaging validation. The results show the effectiveness of radionuclide imaging and the potential of high-order approximation models for BLT reconstruction. Further research will focus on mouse experiments with disease models. In using BLT with these models, validation with FDG-PET may not always be possible if the target tissue does not demonstrate adequate image contrast. For this purpose, we will be utilizing genetically modified mouse models in which target tissues for bioluminescent imaging are expressing both a bioluminescence-based reporter gene and a PET probe/PET reporter gene [16].

Although the simulated and experimental [17] SP_N-based BLT reconstruction algorithm provides improved localization precision of the bioluminescent source, the sensitivity of the detection system of BLT plays a very important role in BLT reconstruction for experimental reconstructions. With the increase of the tumor depth, the optical signals on the surface of the mouse are significantly attenuated. More sensitive detection systems become necessary to improve image reconstruction. A new Optical-PET (OPET) imaging system [18] provides not only the simultaneous detection of optical signals and gamma rays but also higher sensitivity due to the natural multi-view detection mode and the photon collection from larger solid angle. More experiments will be performed on the OPET system, and relevant results will be reported in the future, especially on the effect of signal loss, image reconstruction, and sensitivity for the methodology.

Acknowledgments. We thank Dr. Laurent Bentolila for use of the Maestro 2 system. We are grateful to Judy Edwards and Waldemar Ladno for their assistance with mouse experiments. This work is supported by the NIBIB R01-EB001458, a NIH/NCI 2U24 CA092865 cooperative agreement, DOE DE-SC0001234, and NCI 5-R01 CA08572.

References

1. Ntziachristos V, Ripoll J, Wang LV, Weisslder R (2005) Looking and listening to light: the evolution of whole body photonic imaging. Nat Biotechnol 23(3):313–320
2. Wang G, Li Y, Jiang M (2004) Uniqueness theorems in bioluminescence tomography. Med Phys 31(8):2289–2299
3. Han W, Cong W, Wang G (2006) Mathematical theory and numerical analysis of bioluminescence tomography. Inverse Probl 22:1659–1675
4. Ntziachristos V, Tung C-H, Bremer C, Weissleder R (2002) Fluorescence-mediated tomography resolves protease activity *in vivo*. Nat Med 8(7):757–760
5. Kuo C, Coquoz O, Troy TL, Xu H, Rice BW (2007) Three-dimensional reconstruction of *in vivo* bioluminescent sources based on multispectral imaging. J Biomed Opt 12:024007
6. Wang G, Cong W, Durairaj K, Qian X, Shen H, Sinn P, Hoffman E, McLennan G, Henry M (2006) *In vivo* mouse studies with bioluminescence tomography. Opt Express 14:7801–7809
7. Virostko J, Powers AC, Duco Jansen E (2007) Validation of luminescent source reconstruction using single-view spectrally resolved bioluminescence images. Appl Opt 46:2540–2547
8. Klose AD (2007) Transport-theory-based stochastic image reconstruction of bioluminescent sources. J Opt Soc Am A 24:1601–1608
9. Dehghani H, Davis SC, Jiang S, Pogue BW, Paulsen KD, Patterson MS (2006) Spectrally resolved bioluminescence optical tomography. Opt Lett 31:365–367
10. Alexandrakis G, Rannou FR, Chatziioannou AF (2005) Tomographic bioluminescence imaging by use of a combined optical-PET (OPET) system: a computer simulation feasibility study. Phys Med Biol 50:4225–4241
11. Cong W, Wang G, Kumar D, Liu Y, Jiang M, Wang LV, Hoffman EA, McLennan G, McCray PB, Zabner J, Cong A (2005) Practical reconstruction method for bioluminescence tomography. Opt Express 13(18):6756–6771
12. Mansfield JR, Sowa MG, Mantsch HH (2000) Development of LCTF-based visible and near-IR spectroscopic imaging systems for macroscopic samples. Proc SPIE 3920:99–107
13. Yujie Lu, Machado HB, Douraghy A, Stout D, Herschman H, Chatziioannou AF (2009) Experimental bioluminescence tomography with fully parallel radiative-transfer-based reconstruction framework. Opt Express 17:16681–16695
14. Klose AD, Larsen EW (2006) Light transport in biological tissue based on the simplified spherical harmonics equations. J Comput Phys 220 (1):441–470

15. Benson SJ, Moré J (2001) A limited-memory variable-metric algorithm for bound-constrained minimization. Technical Report ANL/MCS-P909-0901, Mathematics and Computer Science Division, Argonne National Laboratory, Argonne
16. Ray P, De A, Min J-J, Tsien RY, Gambhir SS (2004) Imaging tri-fusion multimodality reporter gene expression in living subjects. Cancer Res 64:1323–1330
17. Lu Y, Douraghy A, Machado HB, Stout D, Tian J, Herschman H, Chatziioannou AF (2009) Spectrally resolved bioluminescence tomography with the third-order simplified spherical harmonics approximation. Phys Med Biol 54:6477–6493
18. Prout DL, Silverman RW, Chatziioannou AF (2004) Detector concept for OPET—a combined PET and optical imaging system. IEEE Trans Nucl Sci 51(3):752–756